Letters

Full-Parameter Identification Model Based on Back Propagation Algorithm for Brushless Doubly Fed Induction Generator

Jingyuan Su, *Student Member, IEEE*, Yu Chen, *Member, IEEE*, Debin Zhang, *Student Member, IEEE*, and Yong Kang

***Abstract*—Brushless doubly fed induction generator (BDFIG) has great potential due to its high reliability and low maintenance cost. To achieve high-performance modeling and control, BDFIG resistances and inductances are necessary. However, the existing identification methods either required professional structure knowledge or special excitations and setups, or only estimated part of parameters. Thus, this letter proposes a multilayer full-parameter identification model based on the back-propagation (BP) algorithm for BDFIG, which is constructed with electric quantities as nodes and parameters as adjustable weights, and utilizes the electric quantities measured from regular operations as data. According to the fitting error obtained by comparing the model outputs with the easily measured references, the BP algorithm is applied to update the weights until the error is sufficiently small. Then, all resistances and inductances can be extracted directly from the weights. Such an identification methodology can be easily embedded into existing BDFIG systems. The simulations and experiments verify its feasibility and accuracy.**

***Index Terms*—Back propagation algorithm, brushless doubly fed induction generator (BDFIG), parameter identification.**

I. Introduction

THE brushless doubly fed induction generator (BDFIG) has great potential in generation applications for its high reliability and low maintenance cost [1], [2]. Its structure is shown in Fig. 1, consisting of the power winding (PW), the control winding (CW), and the closed-structured rotor winding (RW) [3]. The BDFIG generation system is also shown in Fig. 1, where the PW-side converter (PSC) keeps the dc-link voltage $u_{\rm dc}$ stable, and the CW-side converter (CSC) adjusts the BDFIG state [4].

Most of the BDFIG modeling and control strategies highly depended on accurate resistances and inductances [5]–[7]. To obtain these parameters, the existing approaches either calculated them based on detailed structure information, which were direct but led to professional knowledge burdens [8], [9]; or estimated only part of them with approximation, which were simple but the missing parameters may influence the control performance [4], [10]; or obtained them with fitting methods such as least square method and semidefinite programming, which were intuitive but required special excitation [11] or special setup configurations such as no-load [10], open-circuit and short-circuit [12], leading to several setup changes.

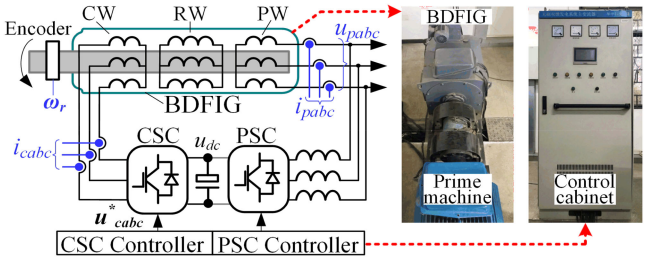

Fig. 1. Common BDFIG generation system.

Considering that the back-propagation (BP) algorithm is a powerful fitting tool especially suitable for multilayer models [13], [14], and the BDFIG model is essentially a group of equations which can be easily turned into a multilayer form, this letter proposes a BDFIG identification model suitable for BP algorithm to obtain all resistances and inductances required by modeling and control. The contributions of this letter are as follows.

1) The multilayer identification model containing the nodes and adjustable weights is specially constructed with clear physical significances, where the nodes correspond to BDFIG currents and voltages, and the weights correspond to BDFIG resistances and inductances.
2) The proposed model takes full advantages of currents and voltages as inputs, and compares its outputs with the measured references for the fitting error. Both inputs and references can be easily measured under regular operations.
3) The BP algorithm is applied to update the weights layer-by-layer according to the fitting error. When the fitting

Manuscript received December 19, 2019; revised January 29, 2020; accepted February 18, 2020. Date of publication February 27, 2020; date of current version June 23, 2020. This work was supported by the National Natural Science Foundation of China under Grant 51777085. *(Corresponding author: Yu Chen.)*

The authors are with the State Key Laboratory of Advanced Electromagnetic Engineering and Technology, Hubei 430074, China, and also with the School of Electrical and Electronic Engineering, Huazhong University of Science and Technology, Hubei 430074, China (e-mail: sujingyuan1991@163.com; ayu03@163.com; zhangdebinbin@163.com; ykang@mail.hust.edu.cn).

Color versions of one or more of the figures in this letter are available online at http://ieeexplore.ieee.org.

Digital Object Identifier 10.1109/TPEL.2020.2976863

error is small enough, all resistances and inductances can be directly extracted from the weights.

Compared with the traditional observer-based approaches, the proposed identification methodology can obtain all BDFIG resistances and inductances synchronously; it utilizes the electric quantities measured under regular operations as data, and thus, specific setup changes such as open-circuit and short-circuit are needless; besides, it is easy to be realized by digital controllers, and thus can be embedded into existing BDFIG systems for online parameter correction. The rest of this letter is organized as follows. Section II illustrates the construction of the BDFIG identification model and the process of the BP-algorithm-based identification; Section III gives both simulation and experimental results to verify the proposed methodology; and Section IV gives the conclusion.

II. BP-Algorithm-Based Identification

A. Review of BDFIG Model

The electric quantities of PW, CW, and RW in BDFIG are in three-phase sinusoidal forms with different amplitudes, frequencies, and phases. To facilitate the analysis and design, the *d–q* rotation coordinate transformation is performed first, and the widely used *d–q* model is given as [2]

$$\text{PW}: \boldsymbol{\psi_p} = L_p\boldsymbol{i_p} + M_{pr}\boldsymbol{i_r} \quad \boldsymbol{u_p} = r_p\boldsymbol{i_p} + s\boldsymbol{\psi_p} + j\omega_p\boldsymbol{\psi_p} \tag{1}$$

$$\text{CW}: \boldsymbol{\psi_c} = L_c\boldsymbol{i_c} + M_{cr}\boldsymbol{i_r} \quad \boldsymbol{u_c} = r_c\boldsymbol{i_c} + s\boldsymbol{\psi_c} - j\omega_c\boldsymbol{\psi_c} \tag{2}$$

$$\text{RW}: \boldsymbol{\psi_r} = L_r\boldsymbol{i_r} + M_{pr}\boldsymbol{i_p} + M_{cr}\boldsymbol{i_c}$$
$$\boldsymbol{u_r} = r_r\boldsymbol{i_r} + s\boldsymbol{\psi_r} + j\omega_{rp}\boldsymbol{\psi_r} \tag{3}$$

where subscripts *p*, *c*, and *r* denote PW, CW, and RW; *r*, *L*, and *M* denote resistance, self-inductance, and mutual inductance; $\boldsymbol{u}$, $\boldsymbol{i}$, and $\boldsymbol{\Psi}$ denote vectors of voltage, current, and flux linkage, formed as $\boldsymbol{x} = x_d + jx_q$ ($\boldsymbol{x}$ stands for $\boldsymbol{u}$, $\boldsymbol{i}$, $\boldsymbol{\Psi}$), and all *d–q* components can be known accurately with the encoder and coordinate transformation [3]; *s* is the Laplace operator; ω_p, ω_c, ω_r, and ω_{rp} denote the electrical frequencies of PW and CW, the rotor speed and the slip frequency, respectively, and have the inherent relations as

$$\omega_c = (p_p + p_c)\omega_r - \omega_p \text{ and } \omega_{rp} = \omega_p - p_p\omega_r. \tag{4}$$

The proposed methodology only requires the voltages and currents measured under regular operations as data, which can be easily obtained under either open-loop or closed-loop control. For a certain operation point, the amplitudes, frequencies, and phases of the three-phase voltages and currents are unchanged. Therefore, the corresponding quantities in the *d–q* coordinate frame are in stable dc forms. With such a precondition, only the steady-state characteristic of the *d–q* model is considered, that is, all derivative terms (*s*-terms) in (1)–(3) are treated as zero. By letting all *s*-terms equal to zero and substituting the left equations of (1)–(3) into the right ones, respectively, the BDFIG model (5)–(7) can be obtained, where u_r is zero due to the closed-structured RW [1]

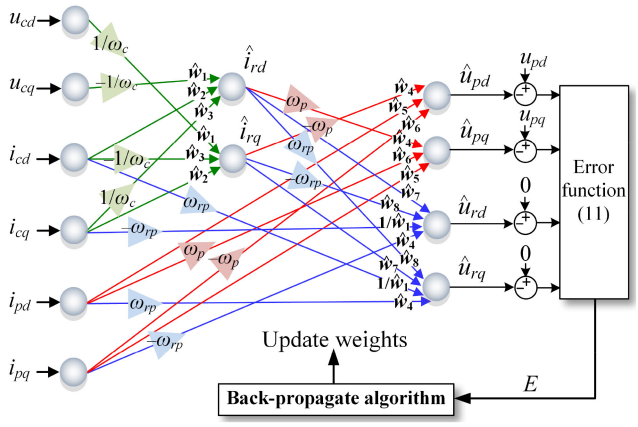

Fig. 2. Multilayer BDFIG identification model.

$$\boldsymbol{u_p} = (r_p + j\omega_p L_p)i_{\boldsymbol{p}} + j\omega_p M_{pr}\boldsymbol{i_r} \tag{5}$$

$$\boldsymbol{u_c} = (r_c - j\omega_c L_c)\boldsymbol{i_c} - j\omega_c M_{cr}\boldsymbol{i_r} \tag{6}$$

$$\boldsymbol{u_r} = 0 = (r_r + j\omega_{rp}L_r)\boldsymbol{i_r} + j\omega_{rp}M_{pr}\boldsymbol{i_p} + j\omega_{rp}M_{cr}\boldsymbol{i_c}. \tag{7}$$

It can be seen that (5)–(7) still contain all eight resistances and inductances (i.e., r_p, r_c, r_r, L_p, L_c, L_r, M_{pr}, and M_{cr}), and thus can be used as the identification basis.

B. Construction of BDFIG Multilayer Identification Model

Considering that the BP algorithm is suitable to update the weights of multilayer models, (5)–(7) are transformed to a multilayer equivalent model first, where BDFIG parameters should be turned into the weights for the BP adjustment. The detailed construction is given as follows.

Layer 1: by splitting (6) into *d–q* form and transforming it slightly, (8) can be obtained as

$$\begin{cases} i_{rd} = -(1/\omega_c)\cdot w_1 u_{cq} - w_2 i_{cd} + (1/\omega_c)\cdot w_3 i_{cq} \\ i_{rq} = (1/\omega_c)\cdot w_1 u_{cd} - w_2 i_{cq} - (1/\omega_c)\cdot w_3 i_{cd} \end{cases} \tag{8}$$

where the weights $w_1 = 1/M_{cr}$, $w_2 = L_c/M_{cr}$, and $w_3 = r_c/M_{cr}$; $1/\omega_c$ is treated as known based on (4); i_{cd}, i_{cq}, u_{cd}, and u_{cq} are naturally taken as input nodes, and i_{rd} and i_{rq} correspond to output nodes.

Based on (8), layer 1 can be built as the green subnetwork shown in Fig. 2, where $\hat{i}_{rd}$ and $\hat{i}_{rq}$ denote the estimated values of i_{rd} and i_{rq}, and will approach i_{rd} and i_{rq} if the weights $\hat{w}_1 - \hat{w}_3$ have been adjusted to approach w_1–w_3, respectively.

Layer 2: Equation (9) can be obtained based on (5) in a similar way as

$$\begin{cases} u_{pd} = -w_4\omega_p i_{rq} + w_5 i_{pd} - w_6\omega_p i_{pq} \\ u_{pq} = w_4\omega_p i_{rd} + w_5 i_{pq} + w_6\omega_p i_{pd} \end{cases} \tag{9}$$

where the weights $w_4 = M_{pr}$, $w_5 = r_p$, and $w_6 = L_p$, and ω_p is treated as known. Then, i_{pd}, i_{pq}, i_{rd}, and i_{rq} are taken as input nodes, and u_{pd} and u_{pq} correspond to output nodes.

Based on (9), layer 2 can be built as the red subnetwork shown in Fig. 2, where $\hat{i}_{rd}$ and $\hat{i}_{rq}$ are provided by layer 1; $\hat{u}_{pd}$ and $\hat{u}_{pq}$ denote the estimated values of u_{pd} and u_{pq}, and will approach u_{pd} and u_{pq} if $\hat{i}_{rd}$ and $\hat{i}_{rq}$ have approached i_{rd} and i_{rq}, and, meanwhile, $\hat{w}_4 - \hat{w}_6$ have approached w_4–w_6, respectively.

Layer 3: similarly, (10) can be obtained based on (7) as

$$\begin{cases} u_{rd} = w_7 i_{rd} - w_8 \omega_{rp} i_{rq} - (1/w_1)\omega_{rp} i_{cq} - w_4 \omega_{rp} i_{pq} \\ u_{rq} = w_7 i_{rq} + w_8 \omega_{rp} i_{rd} + (1/w_1)\omega_{rp} i_{cd} + w_4 \omega_{rp} i_{pd} \end{cases} \tag{10}$$

where the weights $w_7 = r_r$ and $w_8 = L_r$, and ω_{rp} is treated as known based on (4). Then, $i_{cd}, i_{cq}, i_{pd}, i_{pq}, i_{rd}$, and i_{rq} are taken as input nodes, and u_{rd} and u_{rq} correspond to output nodes.

Based on (10), layer 3 can be built as the blue subnetwork shown in Fig. 2, where $\hat{u}_{rd}$ and $\hat{u}_{rq}$ denote the estimated values of u_{rd} and u_{rq}, and will approach u_{rd} and u_{rq} if $\hat{i}_{rd}$, $\hat{i}_{rq}$, $\hat{w}_7$, and $\hat{w}_8$ have approached i_{rd}, i_{rq}, w_7, and w_8, respectively.

Finally, by taking $\hat{i}_{rd}$ and $\hat{i}_{rq}$ as the bonds to connect three layers, the BDFIG multilayer identification model can be constructed as shown in Fig. 2, which is suitable to utilize BP algorithm for fitting purpose. Besides, two merits are gained.

1) The identification model has clear physical significances since parameters are mapped to the weights and the nodes correspond to voltages and currents. Thus, if the outputs $\hat{u}_{pd}$, $\hat{u}_{pq}$, $\hat{u}_{rd}$, and $\hat{u}_{rq}$ fit their actual values sufficiently, all weights naturally approach the actual parameters.
2) The references of $\hat{u}_{pd}$ and $\hat{u}_{pq}$ are the measured u_{pd} and u_{pq}, which can be easily obtained from BDFIG systems (since u_{pd} and u_{pq} have already been sampled for control [6], [7]). The references of $\hat{u}_{rd}$ and $\hat{u}_{rq}$ are the simple zero (since RW is closed-structured). Thus, the model is further simplified.

C. Fitting Principle Based on BP Algorithm

Before realizing fitting, $\hat{w}_1 - \hat{w}_8$ are all set as zero or the empirically estimated values, and thus errors exist between the outputs $\hat{u}_{pd}$, $\hat{u}_{pq}$, $\hat{u}_{rd}$, and $\hat{u}_{rq}$ and the references u_{pd}, u_{pq}, 0, and 0, respectively. Therefore, the error function E is defined as the BP-adjustment criterion

$$E = \frac{1}{2}\left[(u_{pd} - \hat{u}_{pd})^2 + (u_{pq} - \hat{u}_{pq})^2 + (0 - \hat{u}_{rd})^2 + (0 - \hat{u}_{rq})^2\right]. \tag{11}$$

Based on (11) and the principle of BP algorithm, $\hat{w}_1 - \hat{w}_8$ can be updated based on the general formula [13], [14] as

$$\hat{w}_i(k+1) = \hat{w}_i(k) - \eta \cdot \frac{\partial E(k)}{\partial \hat{w}_i(k)} \tag{12}$$

where η is the learning rate, and k and $k+1$ denote the present and the next updates, respectively.

Combined with Fig. 2, the $\hat{u}_{pd}$-node (related to $\hat{w}_4 - \hat{w}_6$) is taken as an example to illustrate the BP adjustment intuitively: 1) the partial derivatives of E to $\hat{w}_4 - \hat{w}_6$ are obtained first based on the chain rule [13], and then $\hat{w}_4 - \hat{w}_6$ can be updated with (12); 2) along the connection of $\hat{w}_4$ to the $\hat{i}_{rq}$-node, since three nodes (related to $\hat{w}_1 - \hat{w}_3$, respectively) exist in the upper layer of $\hat{i}_{rq}$-node, the BP adjustment is continued and $\hat{w}_1 - \hat{w}_3$ are further updated with (12); 3) along the connections of $\hat{w}_5$ and $\hat{w}_6$ to $i_{pd}-$ node and $i_{pq}-$ node, since no node exists in the upper layer, the adjustments of weights in these two branches are finished.

In a similar way, all weights can be updated. After several updates, E is small enough, implying that the model outputs fit their references sufficiently, and thus $\hat{w}_1 - \hat{w}_8$ approach w_1–w_8, respectively. All resistances and inductances can be extracted as follows:

$$\begin{aligned} &r_p = \hat{w}_5,\ r_c = \hat{w}_3/\hat{w}_1, r_r = \hat{w}_7 \\ &L_p = \hat{w}_6, L_c = \hat{w}_2/\hat{w}_1,\ L_r = \hat{w}_8,\ M_{pr} = \hat{w}_4,\ M_{cr} = 1/\hat{w}_1. \end{aligned} \tag{13}$$

III. Simulation and Experimental Verification

The proposed identification methodology is first applied on BDFIG simulation models to verify the feasibility, and then applied on a BDFIG prototype to further verify the validity.

A. Simulation Verification

To verify the feasibility, the 30-kVA BDFIG model is built in MATLAB with parameters in [15] to provide data. Defining $[u_{cd},\ u_{cq},\ i_{cd},\ i_{cq},\ u_{pd},\ u_{pq},\ i_{pd},\ i_{pq}]$ measured from a certain moment as one group of data, the identification model is built in Python, and is adjusted by BP algorithm with several groups, until E is sufficiently small. Then, the identified results are extracted, and the related error e_x is calculated for evaluation as

$$e_x = |x_{\text{iden}} - x_{\text{ref}}|/x_{\text{ref}} \times 100\%,\ x = r_p, r_c \ldots M_{pr}, M_{cr} \tag{14}$$

where x_{iden} and x_{ref} denote the identified results and the parameters used in simulation model, respectively.

In Fig. 3, the BDFIG model is under open-loop control. The amplitude of u_{cabc} sweeps from 2.5 to 30 V with the step of 2.5 V under 900 r/min and 12 Ω load condition (three steps are illustrated in Fig. 3). When the amplitude of u_{cabc} steps, the three-phase i_{cabc}, u_{pabc}, and i_{pabc} are all changed (only u_{pabc} is illustrated in Fig. 3). These electric quantities are transformed to the *d*–*q* coordinate frame (only u_{cdq} and i_{cdq} are illustrated in Fig. 3, and here the *d*-axis is aligned to u_{cd} so u_{cq} is always zero). For each step, a group of data can be measured after the precondition is satisfied (i.e., the BDFIG has been stable at a certain operation point; see the blue crosses in Fig. 3), and totally 12 groups of data with different values can be collected.

In this example, all 12 groups of data are utilized for the BP adjustment, and the learning rate is set as $\eta = 5$ by trial-and-error method (the inputs and weights in our model are not normalized, so the value of η is not between 0 and 1). Case 1 of Fig. 3 gives the tracking performances of all parameters per 25 epochs. It can be seen that error E converges to a small value 9×10^{-2}; meanwhile, all identified parameters extracted from the weights approach their accurate values. It is worth mentioning that, in Case 1, all weights are initialized as zero, so the convergence requires 300 epochs. If the weights are initialized properly, the

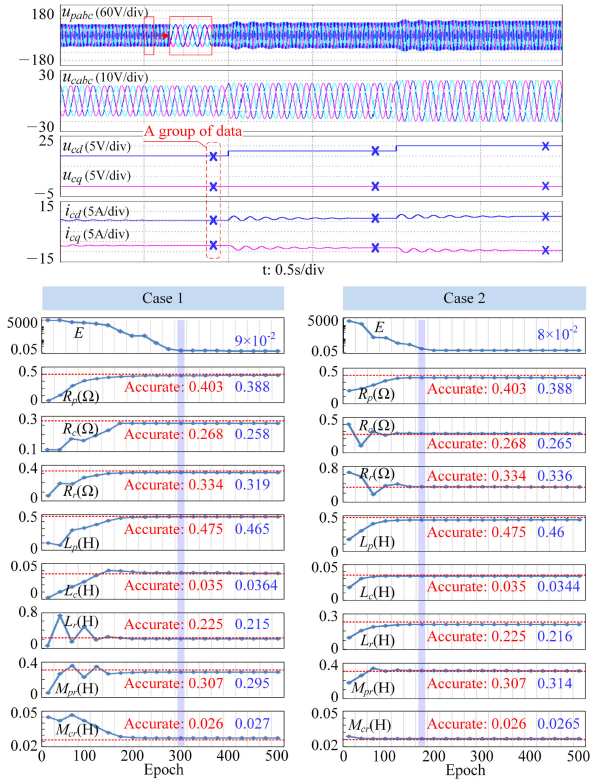

Fig. 3. BP-adjustment process based on open-loop data of the 30-kVA BDFIG.

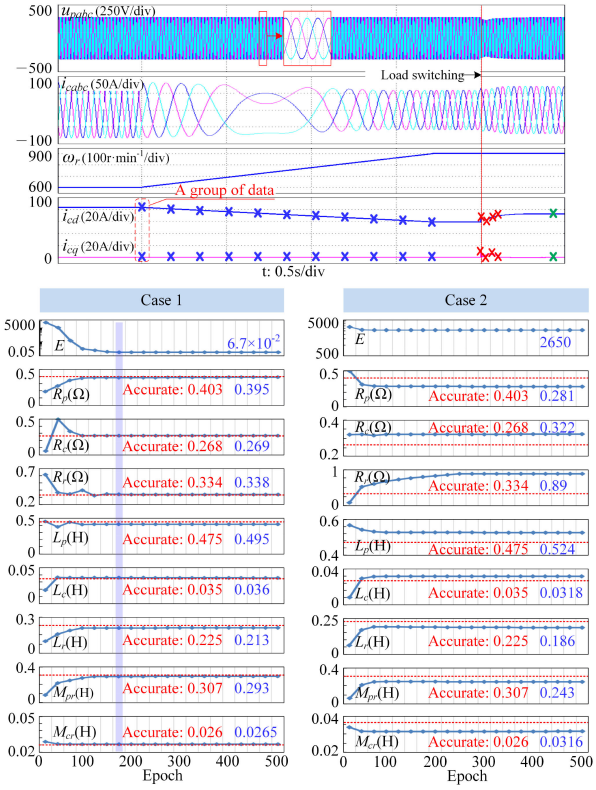

Fig. 4. BP-adjustment process based on closed-loop data of the 30-kVA BDFIG.

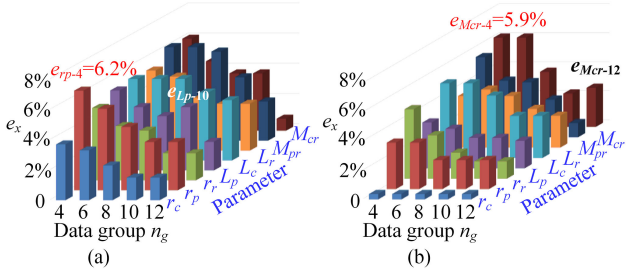

Fig. 5. Identification errors based on 30-kVA BDFIG simulation data. (a) Open loop. (b) Closed loop.

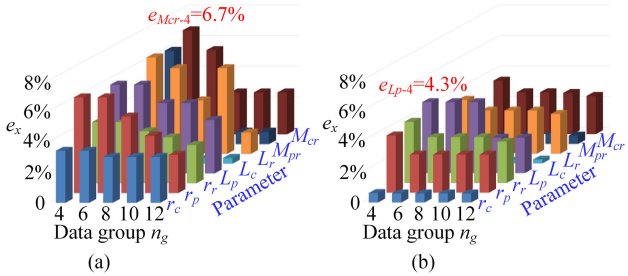

Fig. 6. Identification errors based on 64-kW BDFIG simulation data. (a) Open loop. (b) Closed loop.

convergence could be accelerated. To verify this, in Case 2, the weights are initialized as the empirical values, so all parameters converge to their accurate values after 175 epochs.

In Fig. 4, the BDFIG model is under the stand-alone closed-loop control presented in [4], [16]. Under such a control, the three-phase quantities are transformed to the d–q coordinate frame, and then i_{cd} is regulated for PW voltage control, while i_{cq} is regulated as zero to realize the so-called "forced CW-current orientation." When the rotor speed ω_r varies from 600 to 900 r/min, other electric quantities also vary under the closed-loop effect. Nevertheless, such variations are so slow that their derivative terms can still be treated as zero, and the precondition is still satisfied. Therefore, enough groups of data with different values can be measured during ω_r variation (see the blue crosses in Fig. 4). Besides, after the load is switched and the regulation reaches the stable state, a new group of data can also be measured (see the green crosses in Fig. 4).

Then, the 12 groups of data during ω_r variation and after load switching are utilized for BP adjustment, and the weights are initialized as empirical values. As shown in Case 1 of Fig. 4, all parameters can also converge to their accurate values after 175 epochs, proving the validity of the proposed methodology under closed-loop condition.

For comparison purpose, Case 2 of Fig. 4 shows a counter-example in which the proposed identification methodology fails. In this case, all 12 groups of data are measured during the transient regulation period (see the red crosses in Fig. 4). Since the d–q electric quantities vary fast, the derivative terms cannot be treated as zero, so the precondition is not satisfied. As a result, the error E cannot converge to a small value, and, consequently, all parameters converge to the wrong values.

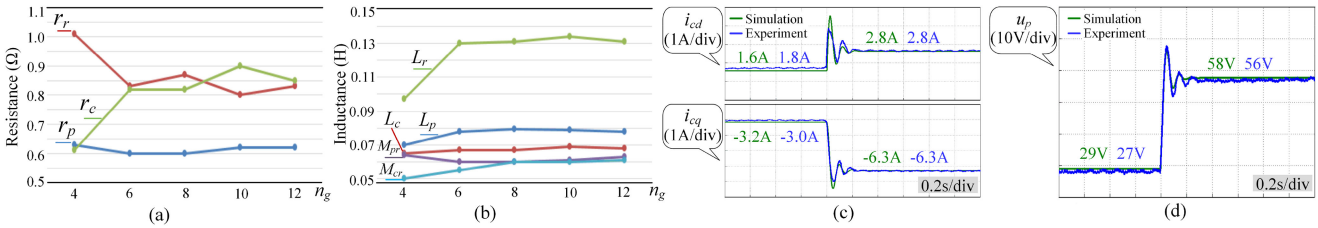

Fig. 7. Identified results based on the experimental data and the open-loop comparisons. (a) Identified results of resistances. (b) Identified results of inductances. (c) Open-loop comparison of $\boldsymbol{i_c}$. (d) Open-loop comparison of $\boldsymbol{u_p}$.

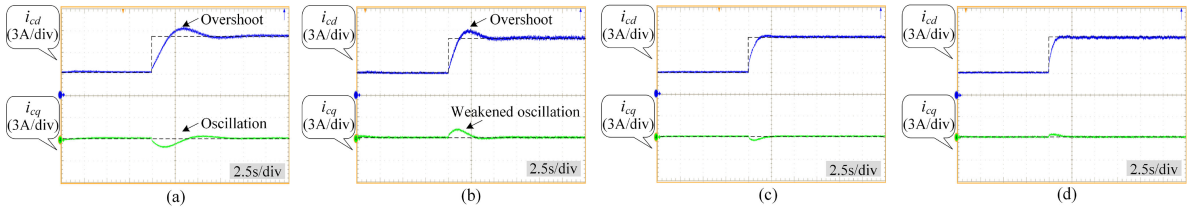

Fig. 8. Comparison of feedforward compensation waveforms. (a) No compensation. (b) Compensation ($n_g = 4$). (c) Compensation ($n_g = 8$). (d) Compensation ($n_g = 12$).

The main difference between the proposed identification model and neural networks is that, neural networks are usually fully connected and with nonlinear activation functions, and thus the local convergence may occur when the training data are inappropriate; however, the proposed identification model is strictly constructed based on the BDFIG model, and no activation function is utilized. Such inherent constrains avoid local convergences largely. Thus, the proposed identification methodology is feasible in the most time of regular operations (except some transient periods such as voltage drop and regulation periods), and suitable for both open-loop and closed-loop controls.

Besides, to evaluate the influence of the data-group number (namely n_g) on identification, 4–12 groups of open-loop and closed-loop data are used for BP adjustment. Then, e_x is calculated based on the identified results and shown in Fig. 5, where the x-axis is n_g; the y-axis denotes the parameters; and the z-axis is e_x. It can be seen that 1) the overall trend of e_x is downward when n_g increases from 4 to 12, implying that the accuracy increases when n_g increases. On the contrary, the identified results may be wrong if n_g is too small (for example, $n_g = 1$ or 2); 2) some local maximal errors can be observed such as e_{Lp-10} in Fig. 5(a) and e_{Mcr-12} in Fig. 5(b), since the BP algorithm only minimizes the total error E, not the individual errors; 3) according to Fig. 5(a) and (b), the e_x based on closed-loop data are close to the open-loop one, further proving that the identification methodology is independent of BDFIG control and thus is robust.

For persuasion, the above process with different n_g is also applied on the 64-kW BDFIG in [10] (the open-loop data are obtained under 400 r/min and 12 Ω load condition; the closed-loop data are obtained when ω_r sweeps from 350 to 650 r/min). As shown in Fig. 6, the phenomena are similar to those of Fig. 5, further verifying the identification validity.

B. Experimental Verification

For further verification, the identification methodology is applied on a wound-rotor BDFIG prototype as shown in Fig. 1, where the 30-kW BDFIG (with 230-V rate voltage and ω_r range as 500 r/min ± 30%) is driven by a prime machine; controllers in the cabinet (with 5-kHz switching frequency) are based on DSP TMS320F28335. It is worth mentioning that the proposed methodology needs not to be implemented at each switching period. Instead, it only runs in the idle time of control routine. Once the BP adjustment is finished, parameters are extracted for control.

Similar to the simulation verification, 4–12 groups of open-loop experimental data (where the amplitude of u_{cabc} sweeps from 2.5 to 30 V with the step of 2.5 V under 400 r/min and 12 Ω load condition) are measured. Based on the data, the identification model is adjusted by the BP algorithm to realize fitting. Such an identification process is realized by DSP within 100 ms. Then, the identified parameters are extracted as shown in Fig. 7(a) and (b). It is seen that when n_g increases to 12, the identified results approach certain stable values, which are close to the actual parameters.

To prove the validity, the identified results with $n_g = 12$ are substituted into the BDFIG simulation model in MATLAB, and the open-loop performances of i_{cd}, i_{cq}, and u_p are compared with those of the prototype under the same condition (where the amplitude of u_{cabc} steps from 10 to 20 V under 400 r/min and 72 Ω load condition) as shown in Fig. 7(c) and (d) (for direct comparison, the experimental waveforms are saved as data first and redrawn in MATLAB). It can be seen that performances of i_{cd}, i_{cq}, and u_p in simulations and experiments match well, verifying the accuracy of the identified results.

Besides, the identified results can provide the parameters required by BDFIG controllers. For example, the feedforward compensation controller in [16] required L_p, L_c, L_r, M_{pr}, and

M_{cr}, which can all be provided by the proposed methodology now. The control performances are given in Fig. 8, where i_{cq} tracks zero and i_{cd} tracks the reference stepping from 3 to 8 A under 400 r/min and 72 Ω load condition. Taking the performance of Fig. 8(a) without compensation as the baseline, it can be seen that: 1) Fig. 8(b) (compensation with results of $n_g = 4$) has better performance compared with the baseline, but the overshoot and oscillations still exist, because the identified results of $n_g = 4$ still have relatively large deviations from the actual parameters; 2) Fig. 8(c) and (d) (compensation with results of $n_g = 8$ and 12, respectively) shows the fast response of i_{cd} without overshoot and the ignorable oscillations on i_{cq}. Thus, it can be concluded that the identified results of $n_g = 8$ and 12 are already close to actual parameters. The above phenomena match the results of the simulation verification.

IV. Conclusion

This letter has proposed a BDFIG multilayer identification model based on the BP algorithm. By comparing $\hat{u}_{pd}$, $\hat{u}_{pq}$, $\hat{u}_{rd}$, and $\hat{u}_{rq}$ calculated based on the measured voltages and currents with actual u_{pd}, u_{pq}, u_{rd}, and u_{rq}, the error function *E* is obtained as the criterion, and the BP algorithm adjusts the weights of the identification model based on *E* to realize fitting. Then, all resistances and inductances required by modeling and control can be extracted from the well-adjusted weights.

Both simulations and experiments verify the feasibility of the proposed methodology. It is seen that the identified results always converge to the actual parameters since the solution space has been constrained by the proposed multilayer model construction. However, the random small errors (0.2%–6.7%) always exist between the identified and actual parameters, because even though the solution space has been constrained, there are still many groups of $\hat{w}_1$–$\hat{w}_8$ satisfying the BP-adjustment termination condition (i.e., *E* is sufficiently small). Nevertheless, such random errors can be neglected since the simulation waveforms based on the identified parameters have matched well with the experimental waveforms, and the feedforward performances have also been improved distinctly with the identified parameters. The proposed methodology can be embedded into both stand-alone and grid-connected BDFIG generation systems, and the idea can also be used to identify the parameters of other models.

References

[1] F. Xiong and X. Wang, "Design of a low-harmonic-content wound rotor for the brushless doubly fed generator," *IEEE Trans. Energy Convers.*, vol. 29, no. 1, pp. 158–168, Mar. 2014.

[2] S. Shao, E. Abdi, F. Barati, and R. A. McMahon, "Stator-flux-oriented vector control for brushless doubly fed induction generator," *IEEE Trans. Ind. Electron.*, vol. 56, no. 10, pp. 4220–4228, Oct. 2009.

[3] L. Sun, Y. Chen, J. Su, D. Zhang, L. Peng, and Y. Kang, "Decoupling network design for inner current loops of stand-alone brushless doubly fed induction generation power system," *IEEE Trans. Power Electron.*, vol. 33, no. 2, pp. 957–963, Feb. 2018.

[4] J. Su, Y. Chen, D. Zhang, and Y. Kang, "Stand-alone brushless doubly fed generation control system with feedforward parameters identification," *IEEE Trans. Ind. Inf.*, vol. 15, no. 11, pp. 6011–6022, Jul. 2019.

[5] J. Poza, E. Oyarbide, D. Roye, and M. Rodriguez, "Unified reference frame dq model of the brushless doubly fed machine," *IEE Proc. Electric Power Appl.*, vol. 153, no. 5, pp. 726–734, Oct. 2006.

[6] M. Kumar, S. Das, and K. Kiran, "Sensorless speed estimation of brushless doubly-fed reluctance generator using active power based MRAS," *IEEE Trans. Power Electron.*, vol. 34, no. 8, pp. 7878–7886, Aug. 2019.

[7] W. Xu, O. M. E. Mohammed, Y. Liu, and M. R. Islam, "Negative sequence voltage compensating for unbalanced standalone brushless doubly-fed induction generator," *IEEE Trans. Power Electron.*, vol. 35, no. 1, pp. 667–680, 2019.

[8] X. Wang, P. C. Roberts, and R. A. McMahon, "Optimisation of BDFM stator design using an equivalent circuit model and a search method," in *Proc. 3rd IET Int. Conf. Power Electron. Mach. Drives*, 2006, pp. 606–610.

[9] S. Yu, F. Zhang, and H. Wang, "Parameter calculation and analysis of a novel wind power generator," *IEEE Trans. Magnetics*, vol. 53, no. 11, pp. 1–7, Nov. 2017.

[10] J. Su, Y. Chen, L. Sun, X. Liu, and Y. Kang, "Parameter estimation of brushless doubly-fed induction generator based on steady experimental results," in *Proc. 2015 IEEE Energy Convers. Congress Expo.*, 2015, pp. 2800–2804.

[11] H. Djadi, K. Yazid, and M. Menaa, "Parameters identification of a brushless doubly fed induction machine using pseudo-random binary signal excitation signal for recursive least squares method," *IET Electric Power Appl.*, vol. 11, no. 9, pp. 1585–1595, Nov. 2017.

[12] P. C. Roberts, R. A. McMahon, P. J. Tavner, J. M. Maciejowski, and T. J. Flack, "Equivalent circuit for the brushless doubly fed machine (BDFM) including parameter estimation and experimental verification," *IEE Proc. Electric Power Appl.*, vol. 152, no. 4, pp. 933–942, Jul. 2005.

[13] W. Lin and C. Hong, "A new elman neural network-based control algorithm for adjustable-pitch variable-speed wind-energy conversion systems," *IEEE Trans. Power Electron.*, vol. 26, no. 2, pp. 473–481, Feb. 2011.

[14] D. Chiozzi, M. Bernardoni, N. Delmonte, and P. Cova, "A neural network based approach to simulate electrothermal device interaction in SPICE environment," *IEEE Trans. Power Electron.*, vol. 34, no. 5, pp. 4703–4710, May 2019.

[15] W. Xu, J. Gao, Y. Liu, and K. Yu, "Model predictive current control of brushless doubly-fed machine for stand-alone power generation system," in *Proc. 43rd Annu. Conf. IEEE Ind. Electron. Soc.*, 2017, pp. 322–327.

[16] Y. Liu, W. Ai, B. Chen, K. Chen, and G. Luo, "Control design and experimental verification of the brushless doubly-fed machine for standalone power generation applications," *IET Electric Power Appl.*, vol. 10, no. 1, pp. 25–35, Jun. 2016.